ADTEC

FINAL REPORT

Contract No. NASW-1603

INTERPLANETARY COMMUNICATIONS STUDY

By

Marvin Cohn, Robert S. Littlepage
and Dennis E. Grimes

ADVANCED TECHNOLOGY CORPORATION
1830 York Road
Timonium, Maryland 21093

Prepared for

HEADQUARTERS
NATIONAL AERONAUTICS AND SPACE ADMINISTRATION
WASHINGTON, D. C. 20546

April 4, 1969

ADVANCED TECHNOLOGY CORPORATION

1830 YORK ROAD TIMONIUM, MARYLAND

A Beckman® SUBSIDIARY

FINAL REPORT

Contract No. NASW-1603

INTERPLANETARY COMMUNICATIONS STUDY

By

Marvin Cohn, Robert S. Littlepage
and Dennis E. Grimes

ADVANCED TECHNOLOGY CORPORATION
1830 York Road
Timonium, Maryland 21093

Prepared for

HEADQUARTERS
NATIONAL AERONAUTICS AND SPACE ADMINISTRATION
WASHINGTON, D. C. 20546

April 4, 1969

TABLE OF CONTENTS

		Page
I.	INTRODUCTION	1
II.	CIRCULAR APERTURE CONSIDERATIONS	2
III.	EXPERIMENTAL VERIFICATION OF THEORETICAL PREDICTIONS	12
IV.	CONCLUSIONS AND RECOMMENDATIONS	23
V.	APPENDIX - ANALYSIS	25

LIST OF ILLUSTRATIONS

Figure	Title	Page
1	Definition of Parameters for the Circular Aperture	5
2	Theoretical Power in the Focal Plane	7
3	Theoretical Power Distribution 1/2 Wavelength in Back of the Focal Plane	8
4	Theoretical Power Distribution 1/2 Wavelength in Front of the Focal Plane	9
5	Comparison of Near Field and Far Field Theoretical Power Patterns for Normal Incidence	10
6	16" Parabolic Reflector with $\frac{f}{D} = 0.25$	14
7	Probe Pattern for .070" Dia. Hole Centered in .5" x .5" Ground Plane	15
8	Focal Plane Probe Covered with Absorber	16
9	Probe Pattern for Two .070" Dia. Holes in a .180" Radius Curved Ground Plane	17
10	Measured Pattern in the Focal Plane (E-Plane)	19
11	Measured Pattern in the Focal Plane (H-Plane)	20
12	Definition of Parameters in Fresnel-Kirchhoff Equation	27
13-a	Incident Wave Vector for a Circular Aperture	29
13-b	Parameters Used in Deriving the Focusing Function δ	29

I. INTRODUCTION

The recent interest in deep space communications, especially satellite-to-earth communications from planetary explorer satellites, has focused attention on improved systems with longer range capabilities. This growing interest in extremely long range communication systems has resulted in the increased use of exceptionally high gain antennas. The desired gains require the use of antennas having very large effective apertures. From the microwave region of the spectrum up through the millimeter wavelengths, there are two basic approaches to achieving large apertures; (1) the use of a single large reflector focused to a feeding element, and (2) the use of an array of smaller apertures whose individual outputs are added.

The primary concern of this program was to examine the parameters and develop a technique for enhancing the efficiency of single large aperture antennas.

II. CIRCULAR APERTURE CONSIDERATIONS

One of the principal parameters in determining the efficiency of an antenna consisting of some reflecting surface is the surface tolerance. By the Rayleigh criterion parabolic reflector surface errors of less than $\lambda/32$ are desired. This tolerance becomes more difficult to maintain as the size of the aperture increases or as the wavelength decreases. These large structures are subject to gravity, wind, and thermal strains all of which are a function of the antenna orientation. Hence, even if one could consider the construction of a perfect antenna, its surface would be distorted during actual operation. Another consideration is that the initial cost of an antenna increases with the required surface tolerance.

A perfect parabolic reflecting surface, illuminated by a uniform plane wave, produces a spherical wave approaching the focal plane. This spherical wave is centered at a collecting aperture in the focal plane. The size of this collecting aperture, commonly called the feed, is adjusted to receive some desired percentage of the total energy in the focal plane. In principle, any deviation from a perfectly spherical aperture distribution will result in less energy collected by the feed. Because of the resulting phase variations in the focal plane, it is felt that rather than simply increasing the size of the collecting aperture, a more efficient technique would be the use of an array of small collecting apertures whose individual phases could be adjusted to maximize their combined output. The total number, position, and relative phase of these collecting apertures is determined by the field structure in the focal plane. An array of collecting apertures will have an advantage only if appreciable energy exists beyond the area covered by the single collecting aperture. This question requires a knowledge of the amplitude and phase

distribution in the focal plane.

ADTEC has performed a study for AFCRL (Contract No. F19628-67-C-0299) to develop a manageable mathematical expression for the phase and amplitude distribution in the focal plane of a large aperture for a reasonably arbitrary distribution in the aperture plane. The aperture plane distribution can be considered to be a result of a number of perturbations, including a distorted reflector surface. The cause of the errors and any time varying effects are not specifically considered in the analysis.

Regardless of the complexity of the aperture plane distribution, a Fourier analysis can be used to reduce the problem to a superposition of plane waves with appropriate phase and amplitude. Because the errors are in general not periodic, a Fourier integral would be required. However, by further analysis and experiment, it could be shown that the effects of very high order waves are negligible and hence an excellent approximation may be achieved with the superposition of some reasonable number of waves.

Once the aperture distribution has been synthesized by an ensemble of plane waves, one must treat the diffraction problem for each individual wave. The antennas of interest have focal length to diameter ratios ($^{f}/D$) less than unity, and in fact a typical value of $\frac{f}{D}$ is 0.25. This represents operation in the near field since the near field - Fresnel boundary occurs at about $\frac{f}{D} = 1.19$ [1]. It can be shown[2] that for apertures large compared to a wavelength, the

1.) John W. Sherman, "Properties of Focused Apertures in the Fresnel Region", IRE Transactions on Antennas and Propagation, Vol. AP-10, No. 4, July, 1962.

2.) E. Wolf and E. W. Marchand, "Comparison of the Kirchhoff and the Rayleigh-Sommerfeld Theories of Diffraction at an Aperture", J. Opt. Soc. Am. 54, 587 (1964).

boundary wave originating from edge currents propagates in the plane of the aperture and hence, except for very large diffraction angles, is negligible. For the apertures of interest and the diffraction angles of interest (limited by the aperture blocking effect) the Fresnel-Kirchhoff scalar diffraction theory is sufficiently accurate. However, the ordinary approximations, such as aperture dimensions being very small compared to the observation distance, cannot be made.

In light of these observations, the Fresnel-Kirchhoff integral was written in a form applicable to the three dimensional problems of interest (Equation numbers apply to the analysis given in the Appendix)

$$U_P = \frac{E_o}{4\pi} \iint \frac{e^{ikr}}{r} \left[\nabla e^{\vec{ik} \cdot \vec{r}'} + ik\delta - ike^{\vec{ik} \cdot \vec{r}'} + ik\delta \hat{r} \right] \cdot \hat{n} dS \quad . \tag{4}$$

where

U_P = wave disturbance at the observation point

$\frac{e^{ikr}}{r}$ = Huygen spherical sources in the aperture

$\vec{k}$ = incident wave vector

$k\delta$ = phase distribution required for focusing

The parameters for the circular aperture are defined in Figure 1. The parameters of the antenna chosen for the experiment were $\frac{D}{\lambda} = 50$ and $\frac{f}{D} = 0.25$.

Equation (4) was studied thoroughly for the circular aperture and the solution is given in the appendix. The resulting expression for the field in the focal plane is,

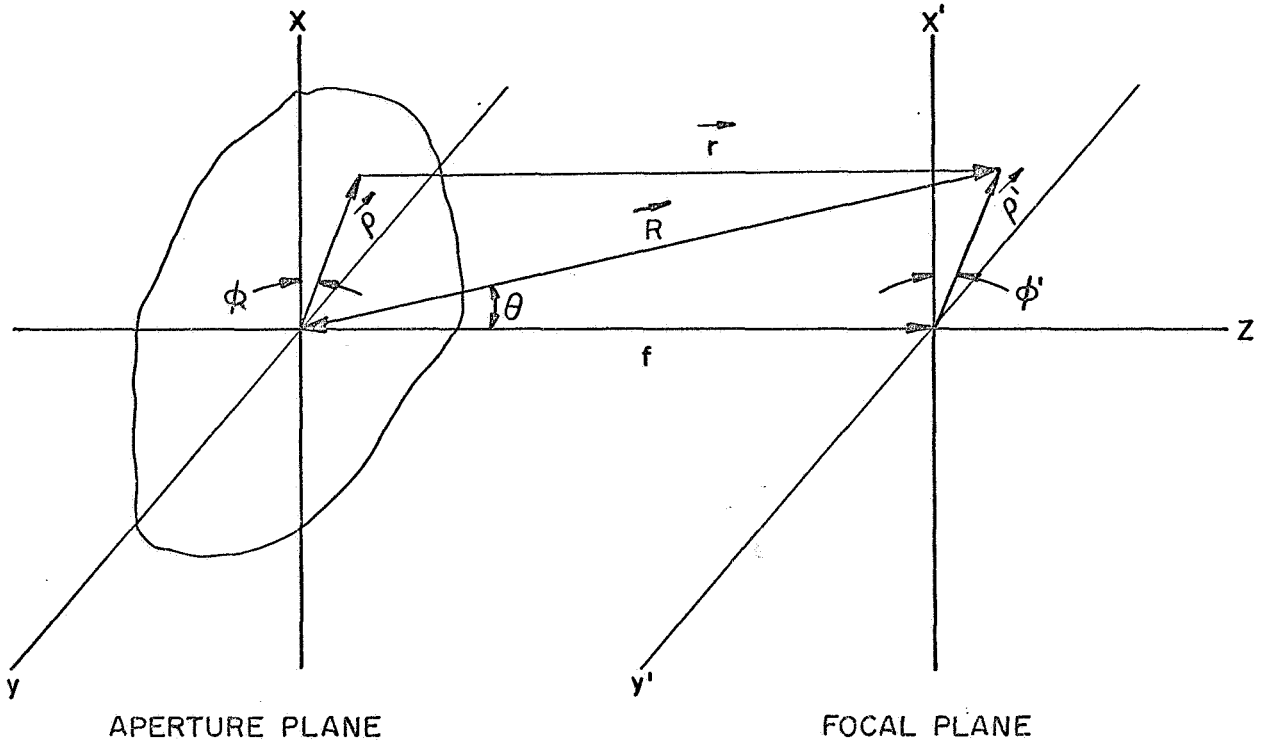

FIG. 1 - DEFINITION OF PARAMETERS FOR THE CIRCULAR APERTURE

$$U_P \approx -\frac{ik}{2} E_o \int_0^{D/2} \frac{e^{ik\left[\left(\frac{f^2}{\cos^2\theta} + \rho^2\right)^{\frac{1}{2}} + \delta(\rho)\right]}}{\left(\frac{f^2}{\cos^2\theta} + \rho^2\right)^{\frac{1}{2}}} J_o\left(k\eta(\rho)\right)\left[\cos\psi + \frac{f}{\left(\frac{f^2}{\cos^2\theta} + \rho^2\right)^{\frac{1}{2}}}\right]\rho\, d\rho \tag{33}$$

where

$$\eta(\rho) = \left[\rho^2 \sin^2\psi + \frac{\rho^2 f^2 \tan^2\theta}{\frac{f^2}{\cos^2\theta} + \rho^2} + \frac{2\rho^2 f \tan\theta \sin\psi \cos(\zeta - \phi')}{\left(\frac{f^2}{\cos^2\theta} + \rho^2\right)^{\frac{1}{2}}}\right]^{\frac{1}{2}}. \tag{32}$$

This integral still requires a numerical computer solution which was performed for $\theta = \pm 20^o$.

Figure 2 is a graph of the computer results of the main beam and first two sidelobes in the focal plane. Figure 3 and Figure 4 indicate the trends of the nulls and sidelobe levels just before and just after the focal plane. It is interesting to note that the depth of the nulls decreases rapidly out of the focal plane. This served as an indicator for locating the focal plane in the experimental verification of the predicted patterns.

A comparison of this Fresnel region field structure with a similar pattern based on the Fraunhofer far field approximation is shown in Figure 5. In the figure, the Fraunhofer pattern is indicated by a broken curve. One must be careful not to make a direct comparison of the absolute value of power between the Fresnel calculations and the Fraunhofer prediction since, although both curves are referenced at the same 0 dB level, in reality the Fraunhofer would peak much lower. This is easily seen by noting that, since the total energy in any plane in front of the aperture is a constant, the area

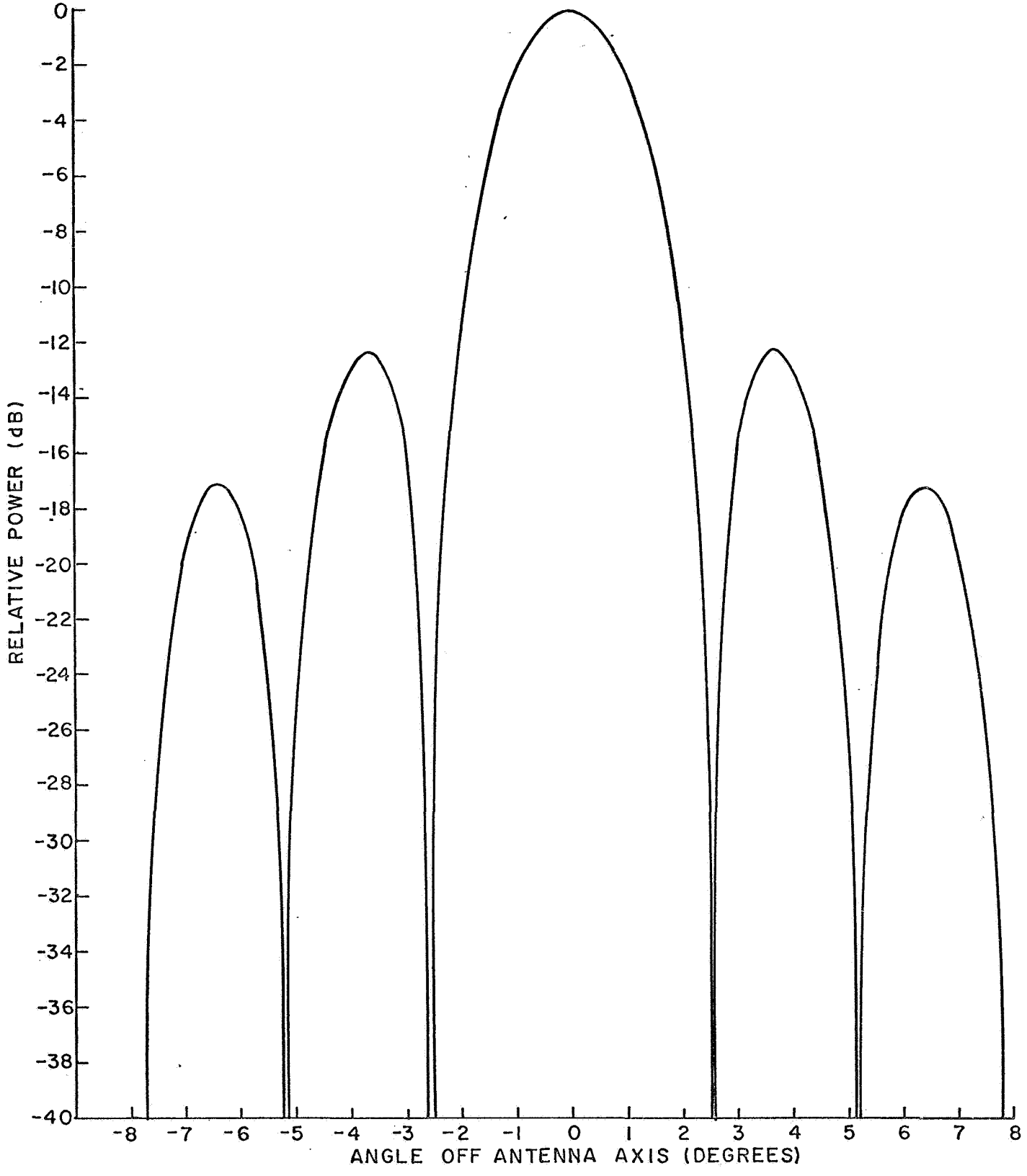

FIG. 2 -THEORETICAL POWER IN THE FOCAL PLANE

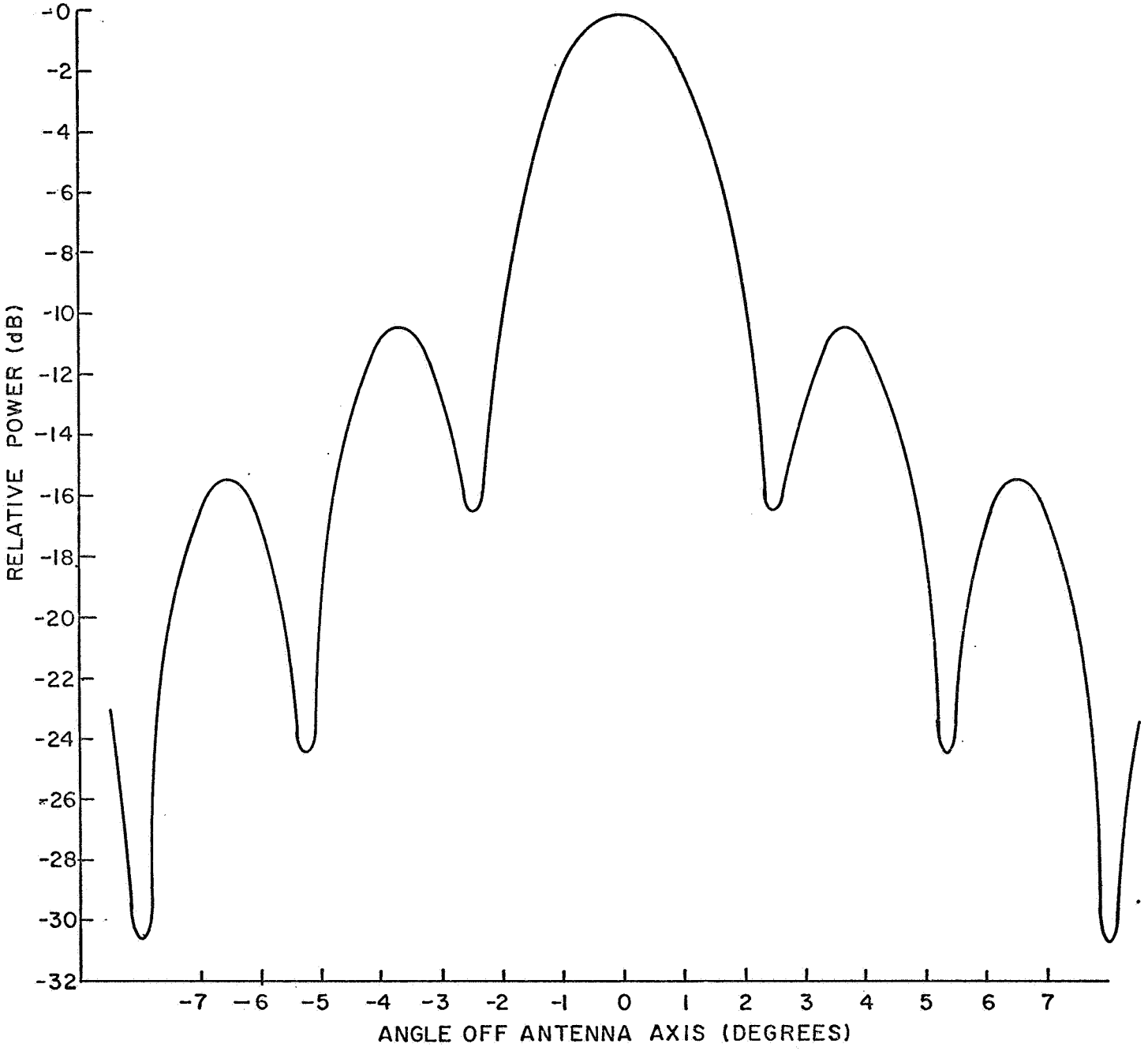

FIG. 3 -THEORETICAL POWER DISTRIBUTION $^{1}/_{2}$ WAVELENGTH IN BACK OF FOCAL PLANE

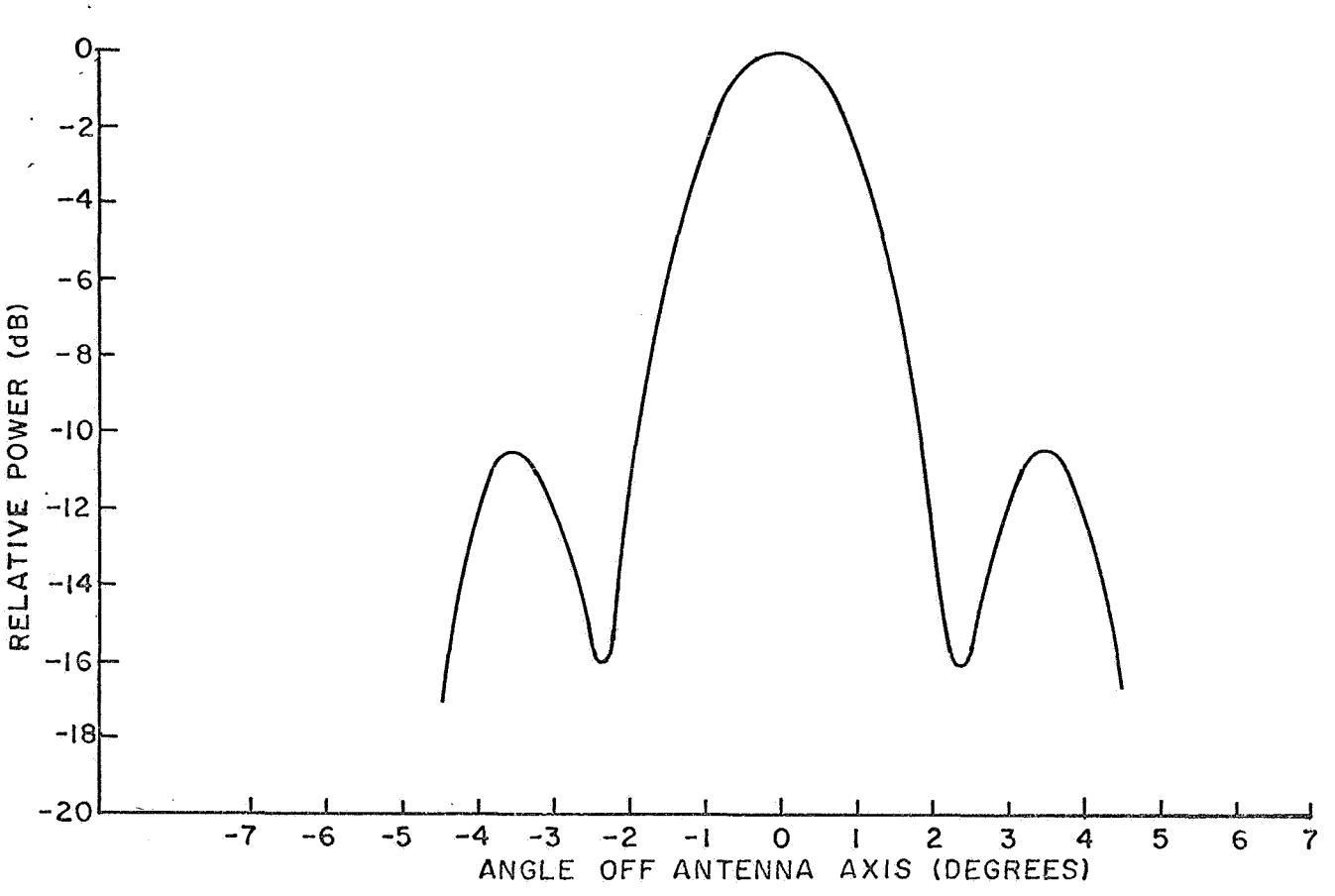

FIG. 4 - THEORETICAL POWER DISTRIBUTION $^1/_2$ WAVELENGTH IN FRONT OF THE FOCAL PLANE

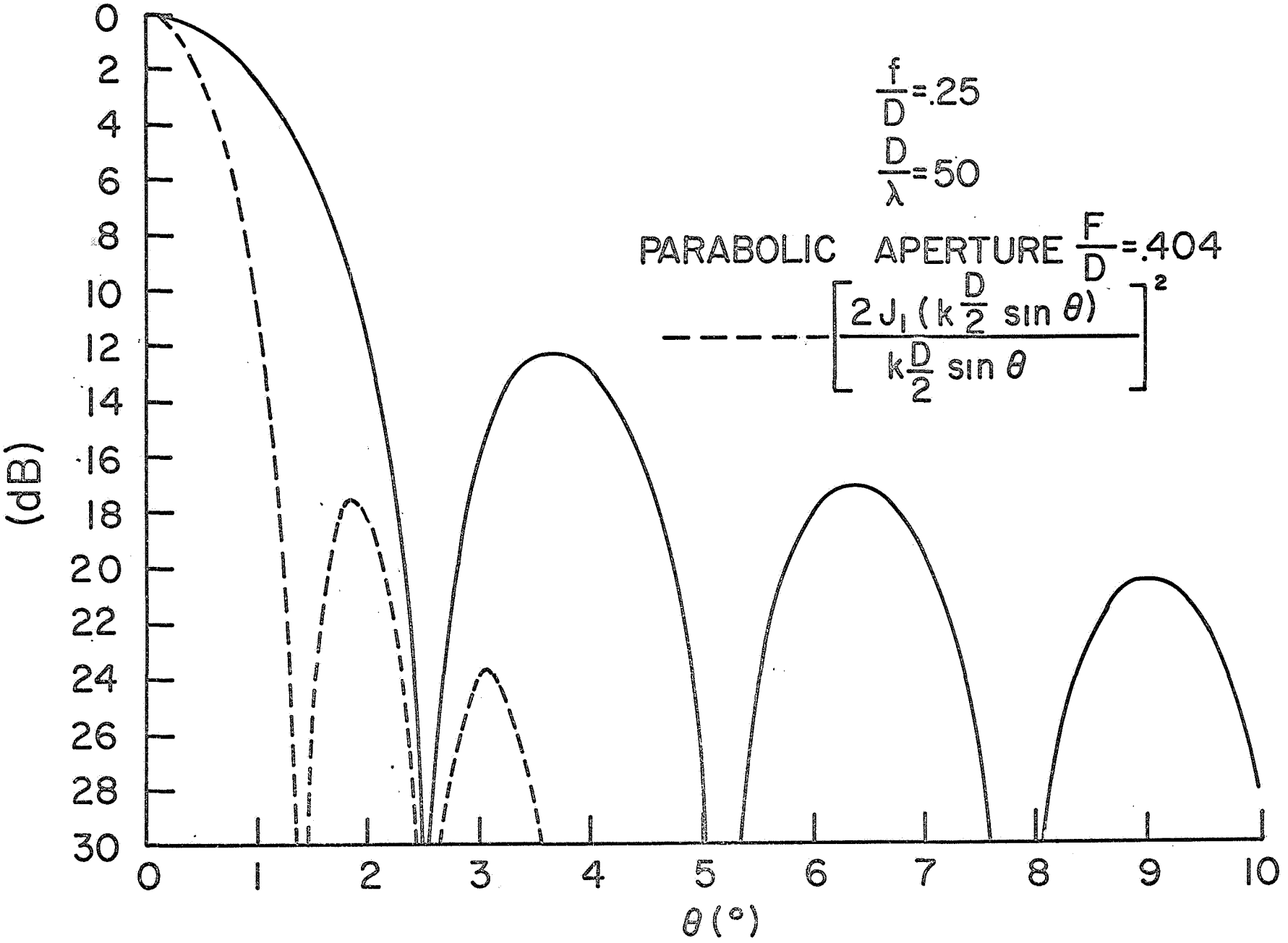

FIG. 5-COMPARISON OF NEAR-FIELD AND FAR-FIELD THEORETICAL POWER PATTERNS FOR NORMAL INCIDENCE

under both curves must be the same. Although the first null of the Fraunhofer pattern is a smaller angular displacement from the axis it must be remembered that the focal plane is a much greater distance from the aperture and, hence, the linear displacement of the first null is actually greater than that for the Fresnel pattern.

The considerable differences between the two patterns emphasizes the importance of knowing the field structure in the Fresnel region when undertaking the design of a feed. For example, a single feed element designed to intercept the Airy disc (central spot) on the assumption that the first null was located at 1.4^{o} would be too small by an angular factor of 1.8 and a considerable loss of power would result.

Calculations have been performed to determine the relative distribution of energy that could be recovered by some multiple element feed system. These calculations are based on the computer results of the field structure in the focal plane of the aperture focused in the near field. These results were plotted ($|E|^2$ vs. angle) and the area under the curve planimetered. It was felt that after seven sidelobes the power (area under the curve) had diminished to such an extent that the addition of more sidelobes would not change the total substantially. Assuming the area under the main beam and the first seven sidelobes to be the total area, the main beam subtends 50.72% of the total. This indicates the maximum efficiency achievable with a single element feed. However, if a multi-element feed were designed to capture the first two sidelobes along with the main beam, the maximum efficiency could be increased to 79.88%. This is a substantial increase and warrants a continued effort on the design of such a feed.

III. EXPERIMENTAL VERIFICATION OF THEORETICAL PREDICTIONS

It was noted in the foregoing analysis that the δ function in Equation 4 was not restricted to any particular physical structure such as a lens or shaped reflector. This section will deal with the definition of a structure to verify the predictions and the experiment itself.

The most readily available and most applicable structure to choose for this effort was the parabola of revolution. Much work has been done on this reflector [3, 4] and extensive study has been made of the related structure, the spherical reflector, by Spencer and Hyde[5]. However some clarification is needed on the notation used. In the previous section f was defined as the distance from the aperture to the focal plane, while the focal length of a parabola of revolution is defined in the literature as the distance from the vertex of the parabola to the focal plane. In order to design a parabolic dish to meet the parameters of the analysis, namely $\frac{f}{D} = 0.25$ and $\frac{D}{\lambda} = 50$ an expression relating f to F, where F is the focal length of the parabola, was needed.

Such an expression is

$$\left(\frac{f}{D}\right)^2 = \left(\frac{F}{D}\right)^2 + \frac{1}{8}\left[\frac{1}{32}\left(\frac{F}{D}\right)^{-2} - 1\right]$$

Using this relationship, $\frac{f}{D} = 0.25$ transforms into $\frac{F}{D} = .404$ for the

---

3. C. J. Sletten and P. Blacksmith, Jr., "The Paraboloid Mirror", Applied Optics, Vol. 4, October 1965.
4. M. S. Afifi, "Radiation From the Paraboloid of Revolution", Electrical Department, Technological University, Delft, The Netherlands.
5. Roy C. Spencer and Geoffrey Hyde, "Transverse Focal Region of a Spherical Reflector", Contract No. AF 19(628)-2748, AFCRL, March, 1964.

parabolic reflector. With this as a criterion, a dish was designed with a 16.0 inch aperture and a focal length of 6.477 inches. For a 50λ aperture, this dictates the frequency to be 36.8 GHz. The parabolic reflector is shown in Figure 6.

In order to measure the field in the focal plane of this reflector, it was necessary to fabricate a probe with an extremely broad radiation pattern. Since the reflector subtends an angle of 126.8^{o} as seen from the focal point, the ideal probe would have a uniform response over this region in both polarizations. Any departure from this is effectively distorting the shape of the reflector. This requirement is impossible to achieve in both planes.

Several probe geometries were tried. A single 0.070 inch hole in a flat ground plane of dimensions 0.5 in. x 0.5 in. was fabricated and tested. The resulting pattern is shown in Figure 7. It is noteworthy that the E-plane pattern has a local minimum on the axis. This was probably due to the radiation of eddy current on the edges of the ground plane. This probe is obviously unacceptable since its sensitivity varies greatly over the angle subtended by the reflector. Reducing the size of the ground plane improved the patterns but a sufficiently broad pattern was not attainable with a flat ground plane.

The probe which was finally decided upon is shown in Figure 8. It consisted of a curved ground plane with two .070 inch radiating holes just off the center line in the H-plane of the waveguide. The measured radiation patterns of the probe are illustrated in Figure 9. The half power beamwidths in the two planes are 103^{o} and 90^{o}. This seemed to be the best approximation to a uniform response of all the probe geometries tried.

With the finalization of the probe design the antenna was ready to be tested. A 225 ft. test range was set up so that the received

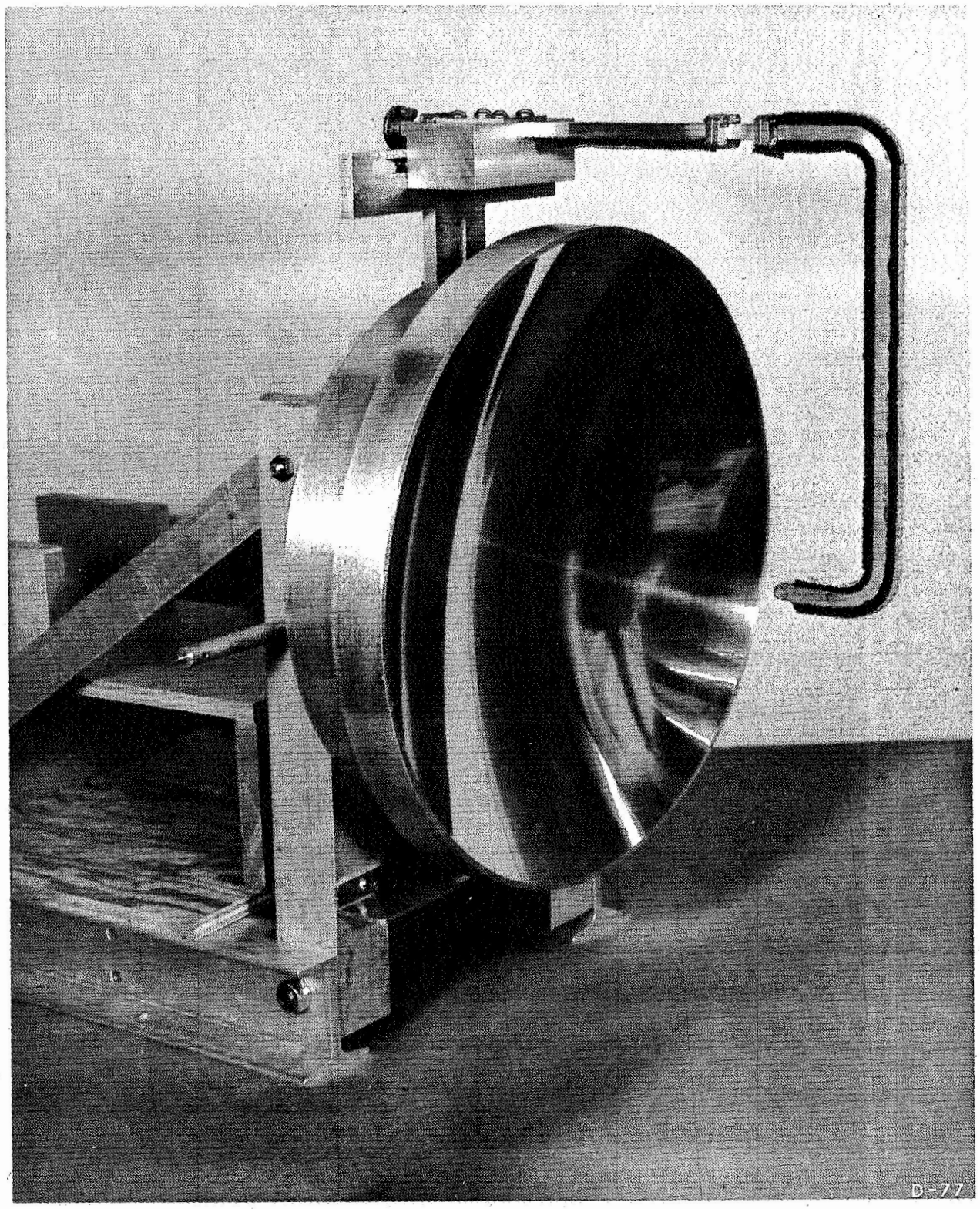

FIG. 6-16" PARABOLIC REFLECTOR WITH $f/D = 0.25$

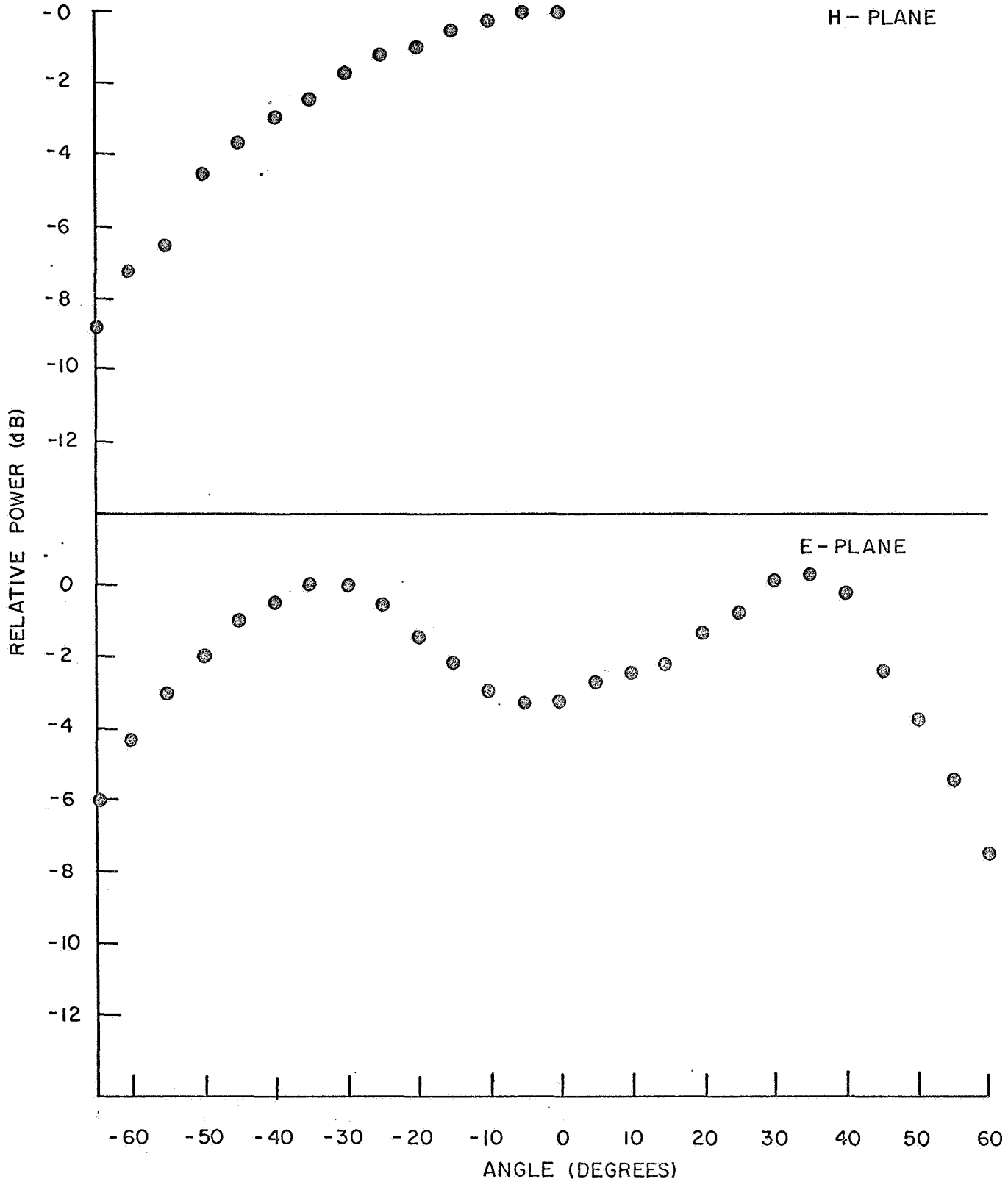

FIG. 7 – PROBE PATTERN FOR .070 DIA. HOLE CENTERED IN .5" X .5" GROUND PLANE

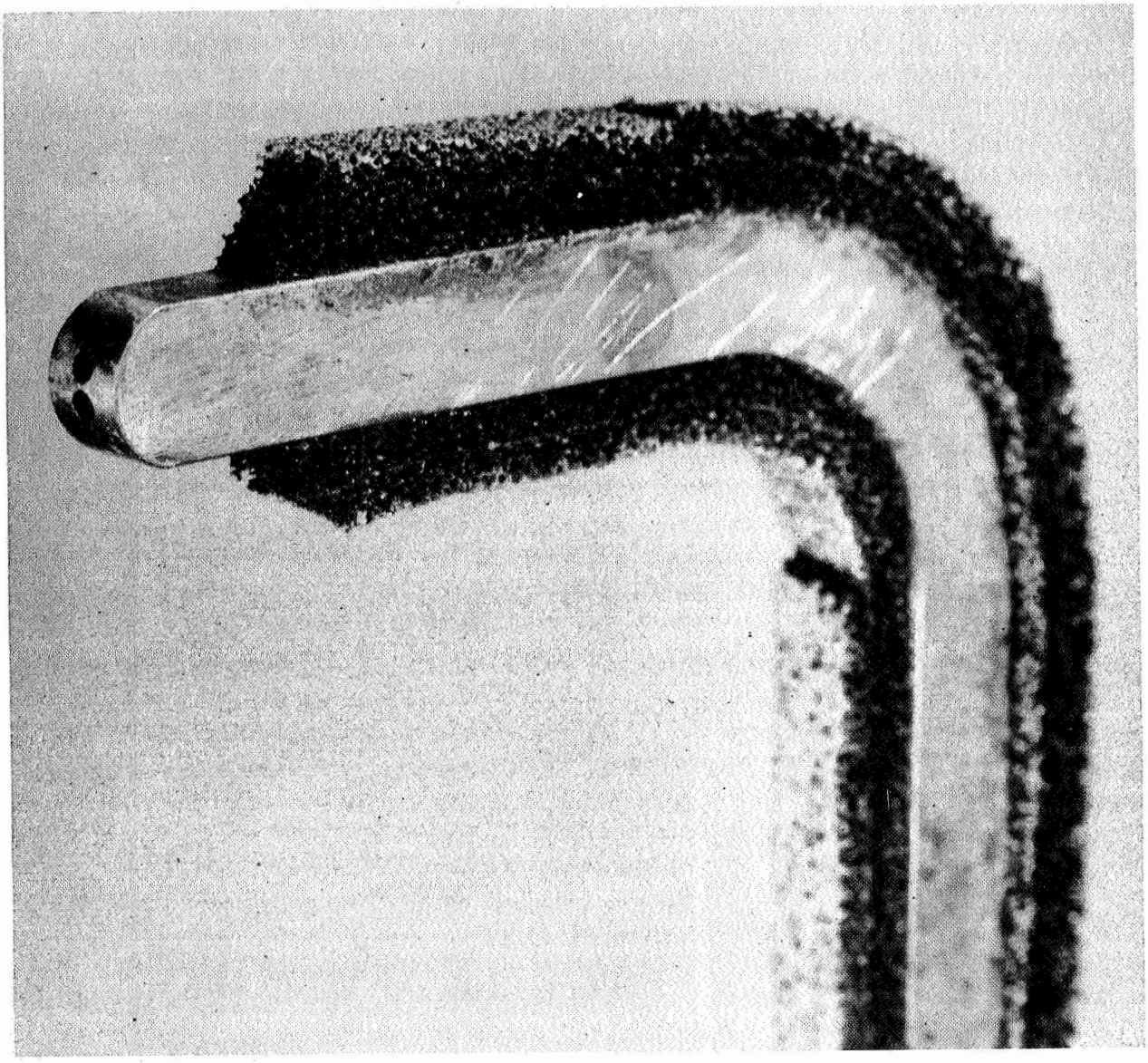

FIG. 8 - FOCAL PLANE PROBE COVERED WITH ABSORBER

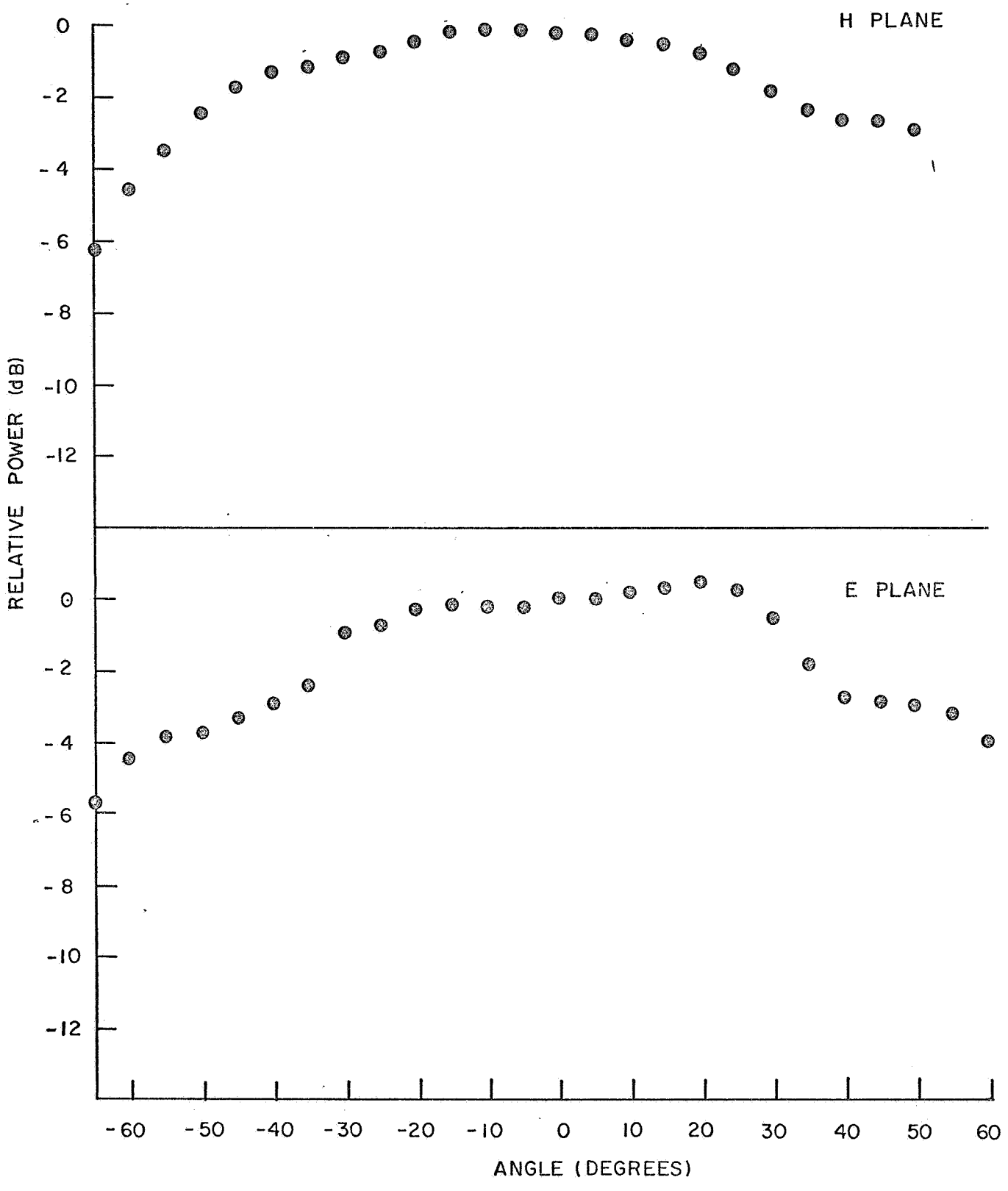

FIG.9 - PROBE PATTERN FOR TWO .070 DIA HOLES IN A .180 RADIUS CURVED GROUND PLANE

could be assumed to be a plane wave. A superheterodyne receiver was used and allowed a 35 dB dynamic range. This capability was sufficient for good definition of the nulls.

The computer results in planes at 13λ and 12λ (with the calculated focal plane at 12.5λ) indicated that the depth of the nulls decreased rapidly outside of the focal plane. This factor was utilized in finding the actual plane of sharpest focus. The probe was positioned at the first null and then moved parallel to the axis of the dish until the deepest null was found. Curiously, the plane of sharpest focus was experimentally found to be at 13λ. Although there are some experimental errors in the measurements, (viz. machining errors on the dish, uncertainty as to the exact location of the phase center of the two hole probe, and edge effects on the diffraction pattern) the cause of this discrepancy is unknown.

The experimental results are graphed in Figures 10 and 11, E-plane and H-plane respectively. A comparison of the E-plane results with the theoretical curve in Figure 2 illustrates that the two curves are in excellent agreement. The theoretical position of the first null is 2.52^{o} off axis, while the measured value is 2.82^{o} -- slightly broader but drastically different from the Fraunhofer prediction of 1.4^{o}. The height of the first sidelobe is 12.3 dB below the main beam in the computer result and 13.3 dB was measured. The second null should have been 5.2^{o} off axis and was found at 5.5^{o}. These results are considered to be in good agreement but a study of the averaging effects of the probe will show that the agreement is even better.

The ideal probe would, of course, have an infinitely small area and would measure power at only one point. In the real world this is not possible, and the size of the hole in the probe is limited by how small the signal can be and still be detected over the range

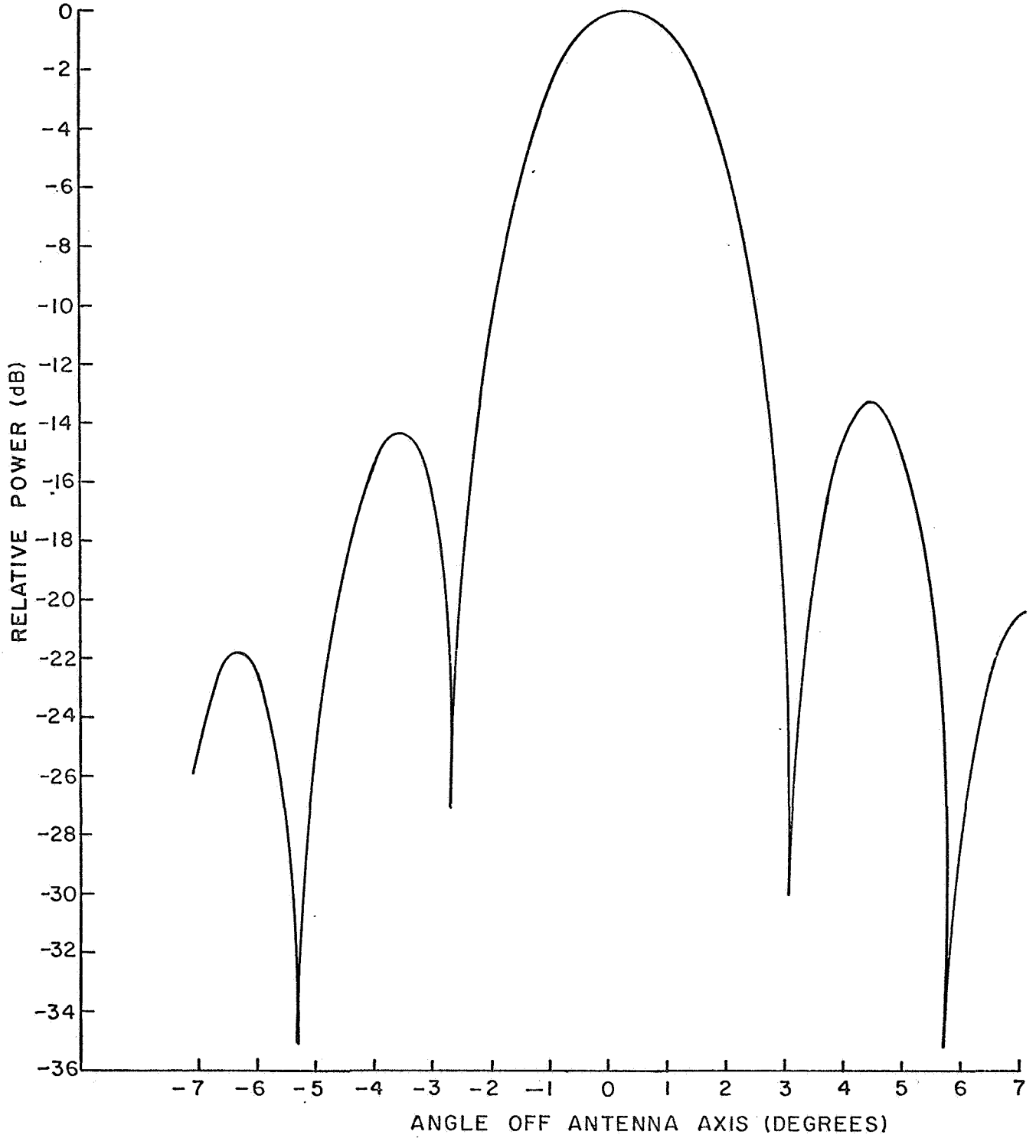

FIG. 10 -MEASURED PATTERN IN THE FOCAL PLANE (E-PLANE)

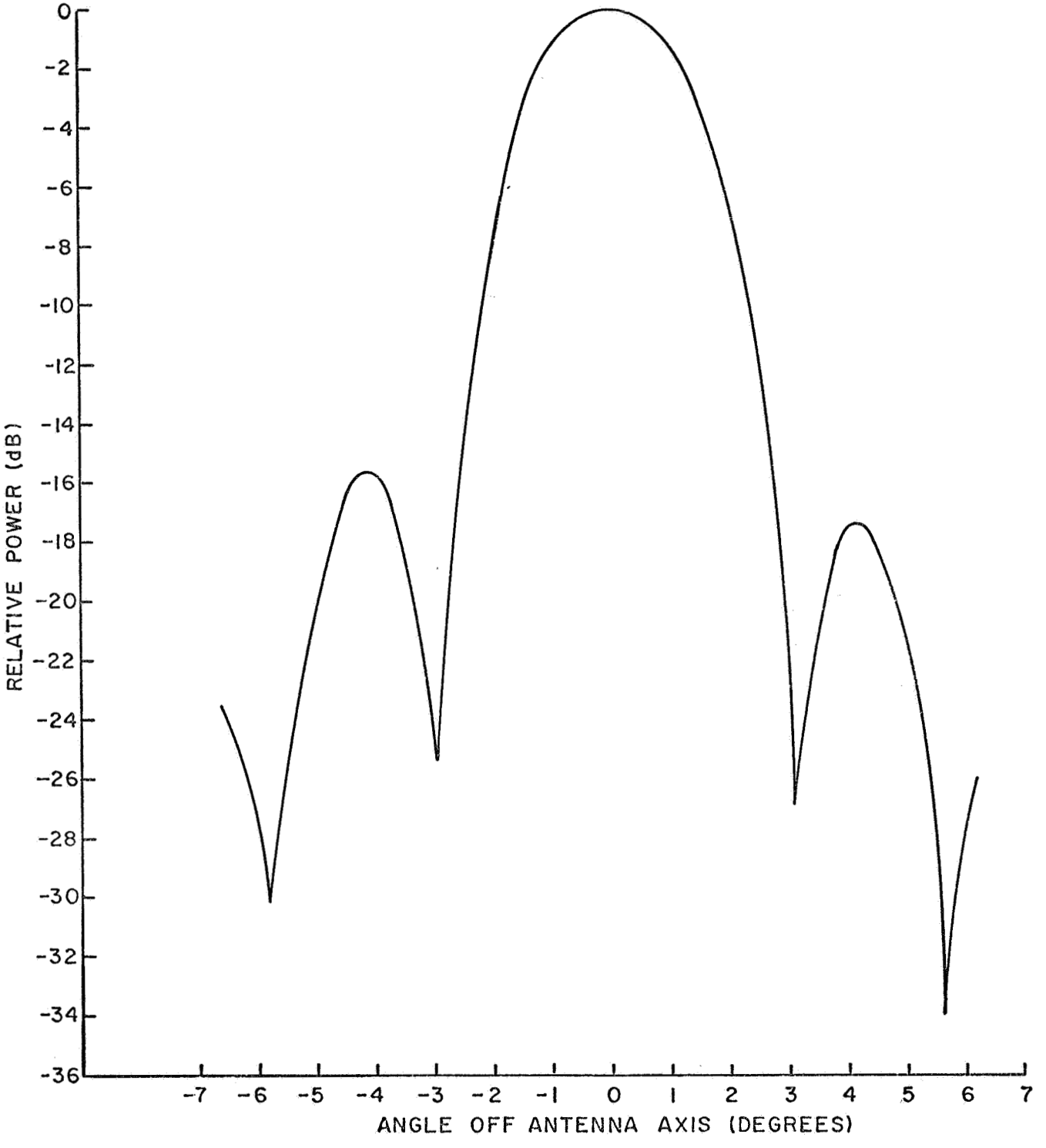

FIG. 11 -MEASURED PATTERN IN THE FOCAL PLANE (H-PLANE)

of values of interest. In this case, the probe had two .070 inch holes as was shown in Figure 8. Although the exact effective area of this arrangement is difficult to pin down, some qualitative analysis is valuable.

In the E-plane of the probe, the cross section of the aperture is .070 inches which subtends about 1^{o} in the focal plane. However in the H-plane, this is increased to 2.2^{o}. In order to examine the effect of this geometry, let us assume that the H-plane aperture consists of two point sources separated by 1^{o} in the focal plane. Then when one of these receiving apertures is situated at the peak of the main beam, the other is seeing the power level at some lower point on the main beam. The result is an average reading. Thus, when the two holes straddle the main beam the resulting measurement is lower than the actual peak value. This condition would be acceptable if it were constant. The same situation on a side lobe (i.e., when the holes are straddling a sidelobe) produces a lower value. This is so because the width of the sidelobe is much less than the width of the main beam and the 1^{o} hole separation positions the holes much lower on the sidelobe.

An effort was made to modify the theoretical results to account for this averaging effect. Two values separated by 1^{o} were averaged at different points along the curve. When the modified curve was redrawn, the width of the main beam was changed from 1^{o} to 1.3^{o} at the 3 dB points. Thus, the beam should have appeared 0.2^{o} wider than the original theoretical values. This makes the measured values only 0.1^{o} off from the theoretical value - well within experimental error. Similarly, the level of the sidelobe in the adjusted theoretical curve was about 14 dB below the main beam and the experimental result in the H-plane was 15.6 dB. Thus, the

correction is improving the agreement of the experimental results. It should be stressed here again that the above analysis is only qualitative since the exact effective area of the probe is not known.

IV. CONCLUSIONS AND RECOMMENDATIONS

The foregoing sections have shown that a workable expression for the field structure in the focal plane for a plane wave illumination can be used to predict these fields. Although the development assumed plane wave illumination (which usually applies to an antenna in the receive mode), the equations are not limited to this case. For example, the $E_o C^{i\vec{k} \cdot \vec{r}}$ of Equation (3) which is used for the plane wave case can be changed to some other distribution like cosine on a pedestal. The field structure necessary to achieve the aperture distribution can then be solved for.

However, it is felt that the case for plane wave illumination will be the most valuable and the benefits which can be derived from the results are legion.

The most immediate benefit from developing an adaptive feed based on the results given in this program is higher antenna efficiency. Higher efficiency for Earth link antennas on Deep Space Probe Satellites is not only desirable but practically a necessity. The lower sidelobe levels which would be effected by adaptive feeding of ground based parabolic antennas makes secure communcation systems easier to achieve. Another important application would be the lowering of the effective antenna temperature on large radiometric antennas. A large part of this noise temperature is due to the sidelobes digging into the hot earth and these sidelobes could be drastically reduced by a focal plane adaptive feed system.

In the light of these observations, it is strongly recommended that efforts be extended toward developing a practical adaptive feed system based on the results of this program. Such a system would be invaluable for many applications.

In addition it is recommended that further analysis be

performed to determine the effects in the focal plane for off axis angles of arrival. The solutions for these angles can then be properly weighted and added to synthesize surface errors in the parabolic reflector. The results of such a study would be especially useful for the design of unfurlable antennas on satellites.

V. APPENDIX - ANALYSIS †

It is felt that, for the majority of antennas of interest, much physical insight can be gained by a more rigorous application of the scalar diffraction theory. This approach neglects polarization effects and hence is only applicable to; (1) the principal polarization in the region of the geometric axis of very large diameter antennas, or (2) for structures which by design permit only a single polarization. The analysis is applicable to a very large class of antennas even if we limit the aperture size to fifty wavelengths or greater ($D/\lambda \geq 50$). It has been shown[6] [7] that for apertures as large as this, the boundary wave due to edge effects has a negligible contribution at moderate diffraction angles, and the Fresnel-Kirchhoff integral represents an excellent approximation to the diffracted fields. For a two dimensional aperture (three dimensional diffraction problem), this integral has the form,

$$U_P = \frac{1}{4\pi} \oint_S \left[\frac{e^{ikr}}{r} \nabla U_S - U_S \nabla \frac{e^{ikr}}{r} \right] \cdot \hat{n} dS, \qquad (1)$$

where

U_P = wave disturbance at the observation point

U_S = wave disturbance at the source point

$\frac{e^{ikr}}{r}$ = Huygen spherical sources in the aperture.

---

6. Wolf, E. and Marchand, E. W., "Comparison of the Kirchhoff and the Rayleigh-Sommerfeld Theories of Diffraction at an Aperture," J. Opt. Soc. Am., 54, 587 (1964).

7. Schivering, F., "On the Range of Validity of Fresnel-Kirchhoff's Approximation Formula," IRE Trans. on Antennas and Propagation, Vol. AP-10, No. 1; January 1962.

† This development was reported by ADTEC in the Final Report for AFCRL Contract No. F19628-67-C-0290.

U_S and $\nabla U_S \cdot \hat{n}$ are taken to be zero everywhere on S except over the region of the aperture. Hence, the integral over the closed surface S reduces to an integral over the aperture. The geometry associated with Equation (1) is shown in Figure 12.

Some simplications can be made to Equation (1), based on the size of the aperture but irrespective of its particular geometry. Consider the term

$$\nabla \frac{e^{ikr}}{r} = \left[-\frac{1}{r} + ik \right] \frac{e^{ikr}}{r} \hat{r} \quad . \tag{2}$$

For the apertures of interest, one can define a range of possible values for the diameter (D), focal length (f), and for the magnitude of the position vector r;

$$50 \leq \frac{D}{\lambda}$$

$$\frac{f}{D} = 0.25$$

$$r \geq f \quad .$$

Considering the poorest case, when $r = f$, one still finds that $k >> {}^{1}/_{r}$ by an amount $6.283 >> 0.08$. Hence, it is reasonable to neglect the term $-{}^{1}/_{r}$ in Equation (2).

We can make some generalizations about the form of U_S. The focusing properties of the aperture will require the inclusion of some phase distribution (a function of the aperture geometry) such that the fields due to every Huygen source add in phase at some distance f along the aperture axis, for a wave with normal incidence at the aperture. The incident field which satisfies these conditions has the form

$$U_S = E_o \, e^{i\vec{k} \cdot \vec{r}' + ik\delta} \quad , \tag{3}$$

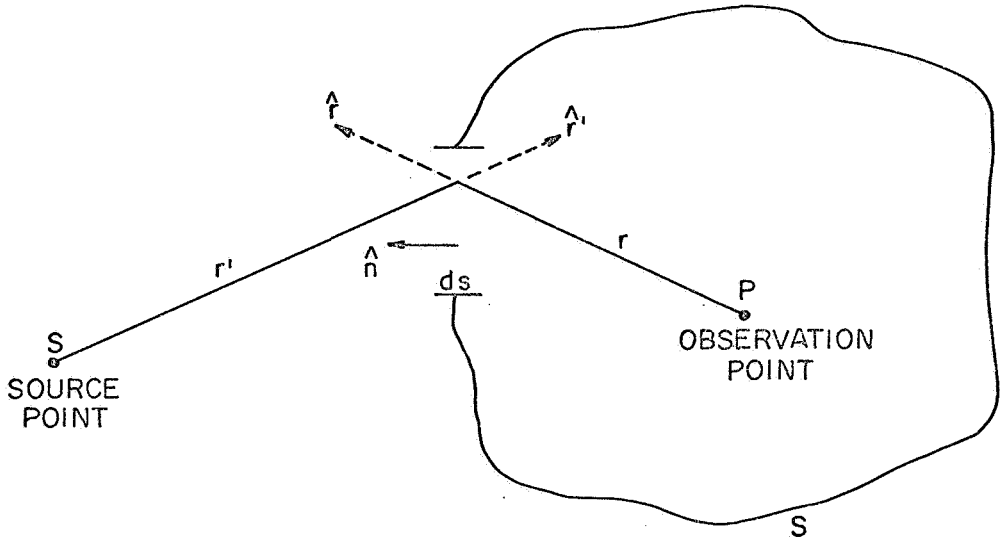

FIG. 12- DEFINITION OF PARAMETERS IN FRESNEL-KIRCHHOFF EQUATION

where

$\vec{k}$ = incident wave vector

$k\delta$ = phase distribution required for focusing.

Equation (1) can now be written in a form applicable to the three dimensional problems of interest;

$$U_P = \frac{E_o}{4\pi} \iint \frac{e^{ikr}}{r} \left[\nabla e^{\vec{ik} \cdot \vec{r'} + ik\delta} - ike^{\vec{ik} \cdot \vec{r'} + ik\delta} \hat{r} \right] \cdot \hat{n} dS \quad . \tag{4}$$

It should be noted that the mechanism for including the focusing property of the aperture is quite arbitrary. It is not restricted to any particular physical structure such as a lens or shaped reflector. Equation (4) has been studied for circular and rectangular apertures.

2.1 Solution of Equation (4) for a Circular Aperture

The incident wave vector $\vec{k}$ is shown for the circular aperture in Figure 13-a. From the figure it is apparent that wave vector for the circular aperture has components of the form

$$k_z = k \cos\psi \tag{5}$$

$$k_x = -k \sin\psi \cos\zeta \tag{6}$$

$$k_y = -k \sin\psi \sin\zeta \quad . \tag{7}$$

The focusing function can be determined by considering the cross-sectional view of the aperture shown in Figure 13-b. Focusing requires that the effective propagation paths, and hence the phase, from every point in the aperture to the point $z = f, \rho' = o$ be the same. This requires that

$$r + \delta = b \text{ (constant)} \tag{8}$$

where

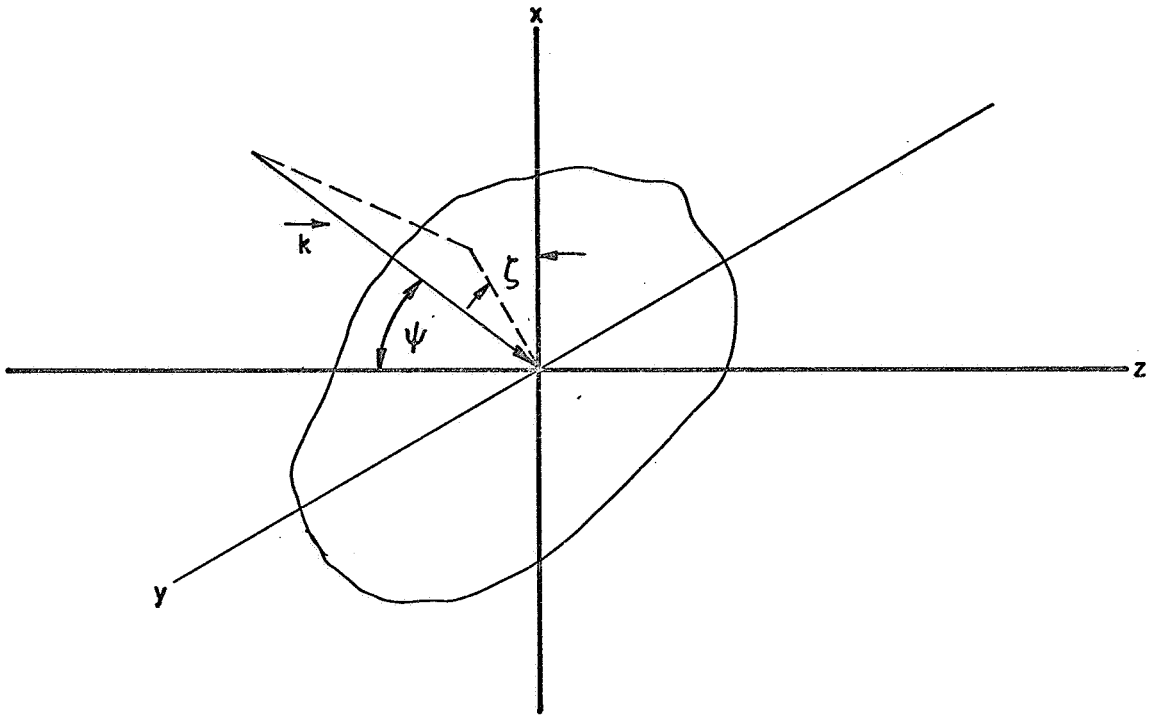

FIG. 13 -a INCIDENT WAVE VECTOR FOR A CIRCULAR APERTURE

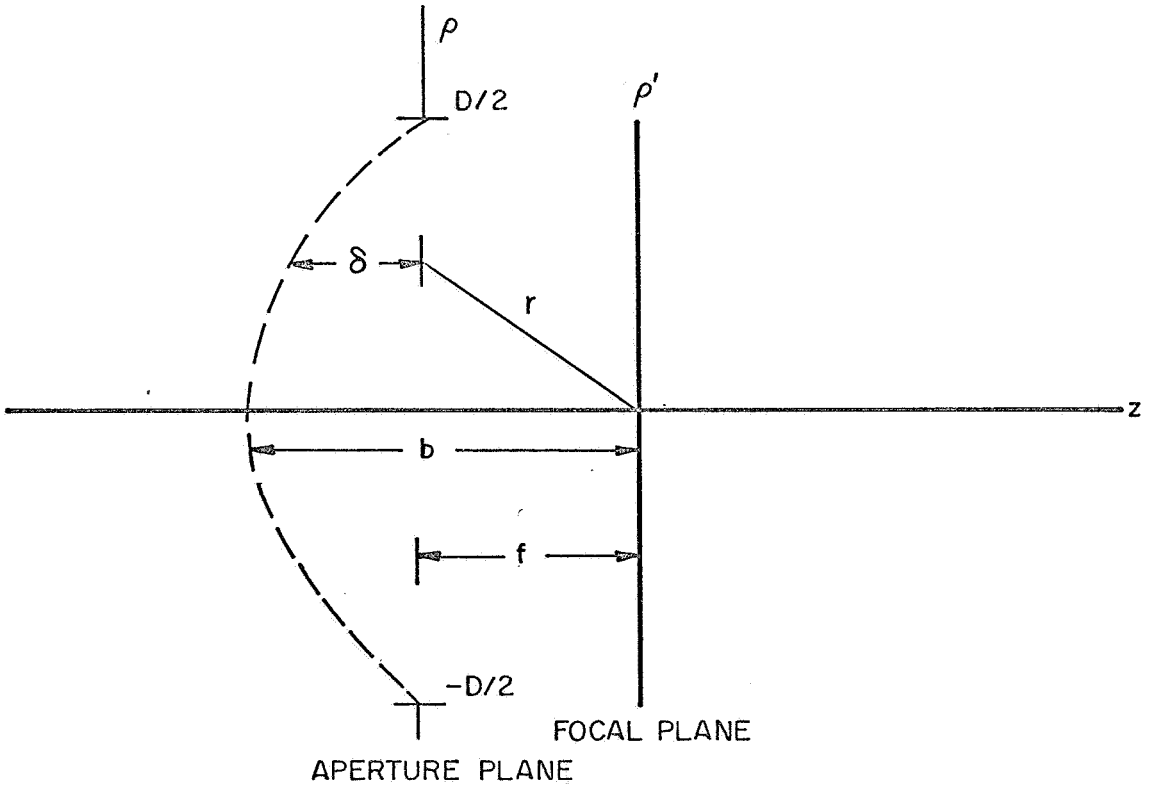

FIG. 13 -b PARAMETERS USED IN DERIVING THE FOCUSING FUNCTION δ

$$b = \left[\left(\frac{D}{2}\right)^2 + f^2\right]^{\frac{1}{2}} \tag{9}$$

and

$$r = \left[\rho^2 + f^2\right]^{\frac{1}{2}} . \tag{10}$$

The focusing function is symmetric in the variable ϕ, and can be found from Equation (8);

$$\delta(\rho) = \left[\left(\frac{D}{2}\right)^2 + f^2\right]^{\frac{1}{2}} - \left[\rho^2 + f^2\right]^{\frac{1}{2}} . \tag{11}$$

Equation (11) does not represent any particular structure, and in fact, when one applies Equation (11) to a particular case care must be taken in defining f and D.

The general definition of the geometric parameters of the circular aperture are given in Figure 1. Under the coordinate transformations,

$$z = z \tag{12}$$

$$x = \rho \cos \phi \tag{13}$$

$$y = \rho \sin \phi , \tag{14}$$

the form of the incident wave, accounting for focusing, becomes

$$U_S = E_o \, e^{ik[z \cos \psi - \rho \sin \psi \cos (\phi - \zeta) + \delta(\rho)]} . \tag{15}$$

The normal component of del operating on U_S is found by taking

$$\nabla U_S \cdot \hat{n} = \left[\frac{\partial U_S}{\partial \rho} \hat{\rho} + \frac{1}{\rho} \frac{\partial U_S}{\partial \phi} \hat{\phi} + \frac{\partial U_S}{\partial z} \hat{k}\right] \cdot \hat{n} \tag{16}$$

where

$$\hat{\rho} \cdot \hat{n} = 0, \; \hat{\phi} \cdot \hat{n} = 0, \; \hat{k} \cdot \hat{n} = -1 . \tag{17}$$

If the aperture plane is defined to be the plane at z = 0, then

$$\nabla U_S \cdot \hat{n} = -ik \cos\psi \, E_o \, e^{ik[-\rho \sin\psi \cos(\phi - \zeta) + \delta(\rho)]} \quad . \qquad (18)$$

Substitution into Equation (4) yields the field due to a circular aperture of diameter D;

$$U_P = \frac{-ik}{4\pi} E_o \int_{\rho=0}^{D/2} \int_{\phi=0}^{2\pi} \frac{F(\rho,\phi)}{r(\rho,\phi)} [\cos\psi + \cos(\hat{n}, \hat{r})] \, \rho d\rho d\phi \qquad (19)$$

where

$$F(\rho,\phi) = \exp[ik(r(\rho,\phi) - \rho \sin\psi \cos(\phi - \zeta) + \delta(\rho))] \qquad (20)$$

$$\cos(\hat{n}, \hat{r}) = \frac{f}{r(\rho,\phi)} \quad . \qquad (21)$$

It is desired to determine the field structure in the focal plane, defined as the plane perpendicular to the z axis through the point z = f. Hence, from Figure 1, the position vector r has the form,

$$r(\rho,\phi) = \left[f^2 + \rho^2 + \rho'^2 - 2\rho\rho' \cos(\phi - \phi') \right]^{\frac{1}{2}} \quad , \qquad (22)$$

and since

$$\rho' = f \tan\theta \qquad (23)$$

one can write

$$r(\rho,\phi) = \left[\frac{f^2}{\cos^2\theta} + \rho^2 - 2\rho f \tan\theta \cos(\phi - \phi') \right]^{\frac{1}{2}} \quad . \qquad (24)$$

Equation (19), with Equations (20), (21), and (24), represents the best expression for the focal plane field structure under the limitations of a scalar approach. The integral cannot be solved in closed form, but requires a numerical computer solution.

In an effort to simplify Equation (19) in order to gain physical insight into the problem, some further approximations can be made. Rewriting Equation (24) in the form

$$r(\rho,\phi) = \left(\frac{f^2}{\cos^2\theta} + \rho^2\right)^{\frac{1}{2}} \left[1 - \frac{2\rho f \tan\theta \cos(\phi - \phi')}{\frac{f^2}{\cos^2\theta} + \rho^2}\right]^{\frac{1}{2}} , \quad (25)$$

and considering only small θ, one can approximate the radical by the first two terms in the binomial expansion;

$$r(\rho,\phi) \approx \left(\frac{f^2}{\cos^2\theta} + \rho^2\right)^{\frac{1}{2}} \left[1 - \frac{\rho f \tan\theta \cos(\phi - \phi')}{\frac{f^2}{\cos^2\theta} + \rho^2}\right] . \quad (26)$$

This approximation will be used in the phase term $\left(F(\rho,\phi)\right)$ of Equation (19). The amplitude terms (terms other than $F(\rho,\phi)$) in Equation (19) can be approximated by

$$r(\rho,\phi) \approx r(\rho) = (f^2 + \rho^2)^{\frac{1}{2}} \quad (27)$$

since they are slowly varying functions of θ. These approximations result in an integrand which is a separable function of ρ and ϕ, and Equation (19) takes the form

$$U_P \approx -\frac{ikE_o}{4\pi} \int_0^{D/2} \frac{F(\rho)\, e^{ik\left[a(\rho) + \delta(\rho)\right]}}{\left(f^2 + \rho^2\right)^{\frac{1}{2}}} \left[\cos\psi + \frac{f}{\left(f^2 + \rho^2\right)^{\frac{1}{2}}}\right] \rho d\rho , \quad (28)$$

with

$$F(\rho) = \int_0^{2\pi} \exp\left[-ik\left(\rho \sin\psi \cos(\phi - \zeta) + \frac{\rho f \tan\theta \cos(\phi - \phi')}{\left(\frac{f^2}{\cos^2\theta} + \rho^2\right)^{\frac{1}{2}}}\right)\right] d\phi \quad (29)$$

and

$$a(\rho) = \left(\frac{f^2}{\cos^2\theta} + \rho^2 \right)^{\frac{1}{2}} . \tag{30}$$

Equation (29) can be solved, and the solution is the zero order Bessel function,

$$F(\rho) = 2\pi J_o \left(k \eta(\rho) \right) \tag{31}$$

where

$$\eta(\rho) = \left[\rho^2 \sin^2\psi + \frac{\rho^2 f^2 \tan^2\theta}{\frac{f^2}{\cos^2\theta} + \rho^2} + \frac{2\rho^2 f \tan\theta \sin\psi \cos(\zeta - \phi')}{\left(\frac{f^2}{\cos^2\theta} + \rho^2 \right)^{\frac{1}{2}}} \right]^{\frac{1}{2}} . \tag{32}$$

The resulting expression for the field in the focal plane is,

$$U_P \approx -\frac{ik}{2} E_o \int_0^{D/2} \frac{e^{ik\left[\left(\frac{f^2}{\cos^2\theta} + \rho^2 \right)^{\frac{1}{2}} + \delta(\rho)\right]}}{\left(\frac{f^2}{\cos^2\theta} + \rho^2 \right)^{\frac{1}{2}}} J_o\left(k\eta(\rho)\right) \left[\cos\psi + \frac{f}{\left(\frac{f^2}{\cos^2\theta} + \rho^2 \right)^{\frac{1}{2}}} \right] \rho d\rho . \tag{33}$$

This integration still requires a numerical computer solution. However, depending on the computer capability, the integration over a single variable may prove to be a valuable simplification.